Gigahertz single source IIR microwave photonic filter based on coherence managed multi-longitudinal-mode fiber laser

Yanbing Jin,[1] Xinhuan Feng,[1,4] Feng Li,[2,*] Xudong Wang,[1] Baiou Guan,[1] Jinhui Yuan,[2,3] and P. K. A. Wai[2]

[1]*Institute of Photonics Technology, Jinan University, Guangzhou, 510632, China*
[2]*Photonics Research Centre, Department of Electronic and Information engineering, The Hong Kong Polytechnic University, Hong Kong SAR, China*
[3]*School of Information and Optoelectronic Science and Engineering, South China Normal University, Guangzhou, 510006, China*
[4]*eexhfeng@gmail.com*
[*]*lifeng.hk@gmail.com*

Abstract: In this paper, we propose to use a multi-longitudinal-mode (MLM) laser as the source of an infinite-impulse response (IIR) microwave photonic filter (MPF) to obtain GHz level free spectral range (FSR). The response function of such an IIR-MPF and the degree of coherence of the laser are discussed theoretically. The degree of coherence of the MLM laser shows a periodic structure which is significantly different to that of single mode lasers. By engineering the degree of coherence of the MLM laser, we are able to control the stability of the IIR-MPFs with different Q factors. It is found that stable IIR-MPF with GHz level FSR can be realized with an MLM laser and its stability can be enhanced if the coherence of the laser is managed. Based on the theoretical analysis, we fabricate an IIR-MPF based on an MLM erbium doped fiber laser. The impacts of the mode spacing Δν and the bandwidth to the stability are investigated experimentally. A stable IIR-MPF with an FSR of 0.59 GHz is realized and the relative fluctuation of the response curve is optimized to be less than 2%. Besides stable response, the IIR-MPF is reconfigurable by tuning the central wavelength of the laser in a range of 20 nm.

OCIS codes: (060.2330) Fiber optics communications; (060.5625) Radio frequency photonics; (070.2615) Frequency filtering.

References and links

1. J. Capmany, B. Ortega, D. Pastor, and S. Sales, "Discrete-time optical processing of microwave signals," J. Lightwave Technol. **23**(2), 702–723 (2005).
2. J. Capmany, B. Ortega, and D. Pastor, "A tutorial on microwave photonic filters," J. Lightwave Technol. **24**(1), 201–229 (2006).
3. R. A. Minasian, "Photonic signal processing of microwave signals," IEEE Trans. Microw. Theory Tech. **54**(2), 832–846 (2006).
4. A. J. Seeds and K. J. Williams, "Microwave photonics," J. Lightwave Technol. **24**(12), 4628–4641 (2006).
5. J. Capmany and D. Novak, "Microwave photonics combines two worlds," Nat. Photonics **1**(6), 319–330 (2007).
6. J. Yao, "Microwave photonics," J. Lightwave Technol. **27**(3), 314–335 (2009).
7. J. Capmany, J. Mora, I. Gasulla, J. Sancho, J. Lloret, and S. Sales, "Microwave photonic signal processing," J. Lightwave Technol. **31**(4), 571–586 (2013).
8. J. Capmany, D. Pastor, and B. Ortega, "New and flexible fiber-optic delay-line filters using chirped Bragg gratings and laser arrays," IEEE Trans. Microw. Theory Tech. **47**(7), 1321–1326 (1999).
9. J. Capmany, J. Mora, B. Ortega, and D. Pastor, "Microwave photonic filters using low-cost sources featuring tunability, reconfigurability and negative coefficients," Opt. Express **13**(5), 1412–1417 (2005).
10. A. P. Foord, P. A. Davies, and P. A. Greenhalgh, "Synthesis of microwave and millimetre-wave filters using optical spectrum-slicing," Electron. Lett. **32**(4), 390–391 (1996).

#227130 - $15.00 USD Received 18 Nov 2014; revised 30 Jan 2015; accepted 1 Feb 2015; published 11 Feb 2015

11. X. Yi and R. A. Minasian, "Noise mitigation in spectrum sliced microwave photonic signal processors," J. Lightwave Technol. **24**(12), 4959–4965 (2006).
12. L. Li, X. Yi, T. X. H. Huang, and R. A. Minasian, "Microwave photonic filter based on dispersion controlled spectrum slicing technique," Electron. Lett. **47**(8), 511 (2011).
13. V. R. Supradeepa, C. M. Long, R. Wu, F. Ferdous, E. Hamidi, D. E. Leaird, and A. M. Weiner, "Comb-based radiofrequency photonic filters with rapid tunability and high selectivity," Nat. Photonics **6**(3), 186–194 (2012).
14. B. Vidal, J. Palací, and J. Capmany, "Reconfigurable photonic microwave filter based on four-wave mixing," IEEE Photon. J. **4**(3), 759–764 (2012).
15. X. Feng, C. Lu, H. Y. Tam, and P. K. A. Wai, "Reconfigurable microwave photonic filter using multiwavelength erbium-doped fiber laser," IEEE Photon. Technol. Lett. **19**(17), 1334–1336 (2007).
16. J. Zhou, S. Fu, F. Luan, J. H. Wong, S. Aditya, P. P. Shum, and K. E. K. Lee, "Tunable multi-tap bandpass microwave photonic filter using a windowed Fabry-Perot filter-based multi-wavelength tunable laser," J. Lightwave Technol. **29**(22), 3381–3386 (2011).
17. J. Abreu-Afonso, A. Díez, J. L. Cruz, and M. V. Andrés, "Continuously tunable microwave photonic filter using a multiwavelength fiber laser," IEEE Photon. Technol. Lett. **24**(23), 2129–2131 (2012).
18. X. Feng, Y. Cao, F. Li, R. Tao, and B. Guan, "Microwave photonic filters based on multi-longitudinal-mode fiber lasers," in *Asia Communications and Photonics Conference 2013*, OSA Technical Digest (Optical Society of America, 2013), paper AW3D.6.
19. E. H. W. Chan, "Suppression of coherent interference effect in an optical delay line signal processor using a single tone phase modulation technique," IEEE Photon. Technol. Lett. **21**(4), 2008–2010 (2009).
20. N. You and R. A. Minasian, "A novel high-Q optical microwave processor using hybrid delay-line filters," IEEE Trans. Microw. Theory Tech. **47**(7), 1304–1308 (1999).
21. B. Ortega, J. Mora, J. Capmany, D. Pastor, and R. Garcia-Olcina, "Highly selective microwave photonic filters based on active optical recirculating cavity and tuned modulator hybrid structure," Electron. Lett. **41**(20), 1133 (2005).
22. J. Mora, B. Ortega, and J. Capmany, "Accurate Control of Active Recirculating Structures for Microwave Photonics Signal Filtering," J. Lightwave Technol. **26**(12), 1626–1631 (2008).
23. E. Xu, X. Zhang, L. Zhou, Y. Zhang, Y. Yu, X. Li, and D. Huang, "Ultrahigh-Q microwave photonic filter with Vernier effect and wavelength conversion in a cascaded pair of active loops," Opt. Lett. **35**(8), 1242–1244 (2010).
24. E. H. W. Chan, "High-Order Infinite Impulse Response Microwave Photonic Filters," J. Lightwave Technol. **29**(12), 1775–1782 (2011).
25. R. Oldenbeuving and P. V. Dijk, "Fully reconfigurable coupled ring resonator-based bandpass filter for microwave signal processing," in *2014 International Topical Meeting on Microwave Photonics (MWP) and the 2014 9th Asia-Pacific Microwave Photonics Conference (APMP),* (2014), pp. 44–47.
26. W. Bogaerts, P. De Heyn, T. Van Vaerenbergh, K. De Vos, S. Kumar Selvaraja, T. Claes, P. Dumon, P. Bienstman, D. Van Thourhout, and R. Baets, "Silicon microring resonators," Laser Photon. Rev. **6**(1), 47–73 (2012).
27. W. Li, W. T. Wang, W. H. Sun, J. G. Liu, and N. H. Zhu, "Microwave photonic notch filter with complex coefficient based on DDMZM," IEEE Photon. Technol. Lett. **26**(18), 1859–1862 (2014).
28. C. L. Chen, "Optical fiber Fabry-Perot cavities and recirculating delay lines as tunable microwave filters," IEEE Trans. Microw. Theory Tech. **38**(5), 647–653 (1990).

1. Introduction

Utilizing microwave photonic signal processing to manipulate radio frequency (RF) signals by photonic techniques has attracted much attention in recent years. By loading onto optical carriers, the RF signals can greatly reduce the transmission loss, enhance the waveguide bandwidth, and benefit from the advanced photonic techniques [1–7]. However, signal processing based on the interference of multiple delayed signal taps, e.g. a microwave photonic filter (MPF), will be sensitive to the optical phases of each signal tap. To avoid the instability caused by the optical interference, most of the reported MPFs are based on incoherent schemes [2]. Optical sources with well separated multiple channels, such as combined laser array [1, 8, 9], spectrum sliced amplified spontaneous emission (ASE) sources including super luminescent diode (SLD) [9–12], frequency comb sources [13], multi-channel source based on four wave mixing (FWM) [14], and multi-wavelength lasers [15–18], can be used as the carriers to avoid the interference. But the multiple sources MPF (MSMPF) with sources covering a large spectral range is incompatible and difficult to be integrated with current wavelength division multiplexing (WDM) systems which should limit the signal in a narrow spectral range. Although the spectral range can be reduced by adopting highly

#227130 - $15.00 USD Received 18 Nov 2014; revised 30 Jan 2015; accepted 1 Feb 2015; published 11 Feb 2015

dispersive fiber [13], such MSMPF is still a finite-impulse response (FIR) system with limited tap number, and cannot generate very high Q factors.

If a single narrowband optical carrier is used in the MPF, although the number of signal taps is no longer limited in the infinite-impulse response (IIR) system, the coherence length of the optical carrier is the dominant factor limiting the design of the system [2, 6, 7]. Since the continuous wave (CW) output from lasers such as distributed feedback (DFB) laser diode (LD) normally has very long coherence length, the time delay T between adjacent signal taps of the IIR-MPF should be large to avoid interference. The large T will limit the free spectral range (FSR) of the MPF response function to very low level. Even with high speed phase modulation to expand the spectral bandwidth of the optical carrier, the FSR of the MPF with such narrowband single source is still limited to far below GHz level [19]. We observe that the high Q factors demonstrated by IIR-MPFs with amplified loops or Fabry-Pérot cavities, and novel high Q resonators are attractive for microwave photonic signal processing [20–26]. Thus it is attractive to design an IIR-MPF with narrowband single source which has large FSR in addition to the intrinsic capability to generate high Q factor. It should also be noted that if a broadband ASE or SLD is used as the optical source in IIR MPF, their short coherence length can push the FSR to large values. However, using more than 10 THz of spectrum to manipulate a signal at ~10 GHz level is clearly undesirable particularly in a WDM system. A narrowband source filtered out from such broad spectra also cannot be used because only a very small portion of power is located in the narrowband which is difficult to be detected.

In this paper, we propose an IIR-MPF with a single source based on multi-longitudinal-mode (MLM) fiber laser. Compared with a broadband ASE or SLD, MLM fiber lasers can generate incoherent signals with much higher power in a narrow bandwidth. The coherence length of the output is much smaller than the DFB LDs benefiting from the large amount of simultaneously lasing longitudinal modes. Thus an IIR-MPF with large FSR can be realized without any active modulation to the optical carrier. The rest of the paper is organized as follows. Section 2 desribes the principle of the IIR-MPF based on an MLM laser and coherence management of such a laser. IIR-MPF with GHz level FSR based on such MLM fiber laser is experimentally demonstrated in Section 3. We conclude the paper in Section 4.

2. Principle of IIR-MPF based on multi-longitudinal-mode lasers

2.1 IIR-MPF and the coherence of source

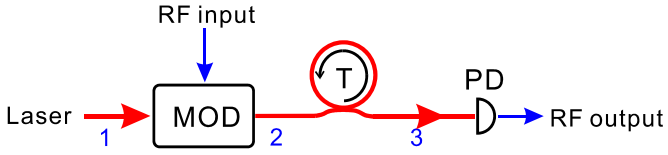

Fig. 1. Schematic of an IIR MPF. MOD: modulator, PD: photodiode, T: Tap generator with time delay T.

The schematic of an IIR-MPF is shown in Fig. 1 [2, 24]. The modulator will load the RF input signal onto the laser carrier before it is injected into the tap generator which can be a fiber loop or other kind of optical resonator. The tap generator will generate multiple taps of the MPF with identical time delay T. The laser signal will finally be converted back into RF signal by the photodiode. For a given laser source, the output signal can be described by the complex amplitude $\tilde{E}_1(\nu)$ in frequency domain. The detected signal amplitude in time domain at point 3 can be written as [2],

$$E_3(t) = \sum_{n=0}^{N} K_n A(t - nT) \int_{-\infty}^{+\infty} \tilde{E}_1(\nu) e^{i2\pi\nu(t-nT)} d\nu \qquad (1)$$

#227130 - $15.00 USD Received 18 Nov 2014; revised 30 Jan 2015; accepted 1 Feb 2015; published 11 Feb 2015

where $A(t)$ is the amplitude variation induced by the RF modulation and K_n is the amplitude factor representing the relative amplitude of the output signal of the n-th tap from the tap generator. The output RF signal of the photodiode (PD) is proportional to the intensity of the optical signal at point 3 as,

$$\begin{aligned} I_3(t) &= E_3^*(t)E_3(t) \\ &= \sum_{n=0}^{N}\sum_{m=0}^{N} K_n K_m A(t-nT)A(t-mT)\int_{-\infty}^{+\infty}\int_{-\infty}^{+\infty}\tilde{E}_1^*(\nu)\tilde{E}_1(\nu')e^{i2\pi\nu'(t-mT)-i2\pi\nu(t-nT)}d\nu d\nu'. \end{aligned} \tag{2}$$

For lasers with continuous wave output, where the phases of the complex amplitude $\tilde{E}_1(\nu)$ with different frequencies ν are uncorrelated, the integration of the cross term $\tilde{E}_1^*(\nu)\tilde{E}_1(\nu')$ will be zero for $\nu \neq \nu'$. Let the central frequency of the signal spectrum is at ν_0, the intensity can be written as:

$$\begin{aligned} I_3(t) &= \bar{I}_1\sum_{n=0}^{N} K_n^2 A^2(t-nT) \\ &+\bar{I}_1\sum_{n=0}^{N}\sum_{m\neq n,m=0}^{N} K_m K_n A(t-mT)A(t-nT)\exp[i2\pi\nu_0(n-m)T]\Gamma[(n-m)T], \end{aligned} \tag{3}$$

where $\bar{I}_1 = \int_{-\infty}^{+\infty}\left|\tilde{E}_1(\nu)\right|^2 d\nu$ is the average intensity of the output signal from the laser and $\Gamma[(n-m)T]$ is the complex degree of coherence of the laser signals with time delay $(n-m)T$ which is calculated from the power spectrum of the signal according to the Wiener-Khinchin theorem as

$$\Gamma(t) = \frac{1}{\bar{I}_1}\int_{-\infty}^{+\infty}\left|\tilde{E}_1(\nu)\right|^2 e^{i2\pi(\nu-\nu_0)t}d\nu = \mathscr{F}^{-1}[I(\nu-\nu_0)]/\bar{I}_1. \tag{4}$$

In Eq. (3), the first term is independent of the temporal variation of the laser signal but the factor $\exp[i2\pi\nu_0(n-m)T]$ in the second term is sensitive to the variation of the time delay T. The second term can be neglected only if the corresponding values of $K_mK_n\Gamma[(n-m)T]$ are small for all values of m and n. Thus the $\Gamma(t)$ function of the optical source is the dominant parameter that determines the stability of the intensity in Eq. (3). From Eq. (3), if all coherent terms vanish, the remaining first term will show a stable response of the filter. The remaining term of the incoherent filter will always have positive coefficient which will limit the performance of the filter [2]. Additional manipulation such as dual modulation would then be required to realize complex coefficient MPF based on the incoherent scheme [2, 27].

To investigate the coherence of different types of light source, here we discuss the degree of coherence of the signals from (a) single mode lasers, (b) MLM lasers, and (c) filtered white noise source. The spectra of the three types of signals can be described by

$$I_a(\nu-\nu_0) = \delta(\nu-\nu_0)\otimes\exp(-\nu^2/\nu_l^2), \tag{5}$$

$$I_b(\nu-\nu_0) = \exp[-(\nu-\nu_0)^2/\nu_s^2]\times\sum_{k=-\infty}^{+\infty}\delta(\nu-\nu_0+k\Delta\nu)\otimes\exp(-\nu^2/\nu_l^2), \tag{6}$$

$$I_c(\nu-\nu_0) = \exp[-(\nu-\nu_0)^2/\nu_s^2], \tag{7}$$

where δ is the Dirac delta function, ν_l is the linewidth of the single mode laser or of each individual mode in MLM lasers. Δν is the mode spacing of the MLM laser. The bandwidth of the spectral envelope of the MLM laser and the filtered white noise are assumed to be

#227130 - $15.00 USD Received 18 Nov 2014; revised 30 Jan 2015; accepted 1 Feb 2015; published 11 Feb 2015

identical to ν_s. The complex degree of coherence $\Gamma(t)$ of such signals can be calculated by Eq. (4) as

$$\Gamma_a(t) = \exp(-\pi^2 \nu_l^2 t^2), \tag{8}$$

$$\Gamma_b(t) = \exp(-\pi^2 \nu_s^2 t^2) \otimes \sum_{k=-\infty}^{+\infty} \delta(t + k/\Delta\nu) \times \exp(-\pi^2 \nu_l^2 t^2), \tag{9}$$

$$\Gamma_c(t) = \exp(-\pi^2 \nu_s^2 t^2). \tag{10}$$

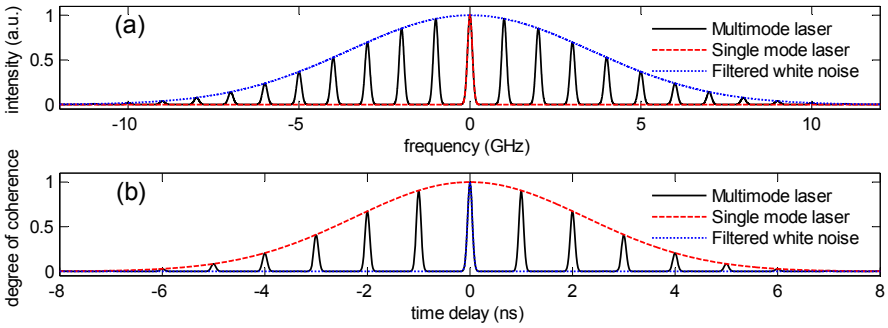

Fig. 2. (a) The spectra and (b) the corresponding degree of coherence versus time delay for an MLM laser (black solid curves), single mode laser (red dashed curves), and filtered white noise source (blue dotted curves).

Figure 2 shows the spectra and corresponding degree of coherence $\Gamma(t)$ versus time delay of the three types of signals with ν_l = 0.1 GHz, ν_s = 5 GHz and $\Delta\nu$ = 1 GHz. The line shape of each individual mode of the MLM laser is similar to the line shape of single mode laser but with different intensities. The mode intensity envelope of the MLM laser overlaps the spectrum of the filtered white noise. From Fig. 2(b), the degree of coherence of the MLM laser $\Gamma_b(t)$ shows a periodic profile with period $1/\Delta\nu$. The envelope of the periodic peaks overlaps the $\Gamma_a(t)$ function of the single mode laser. All the periodic pulses of $\Gamma_b(t)$ have similar profile as the $\Gamma_c(t)$ function but with different intensities. Such a unique periodic structure of the $\Gamma_b(t)$ function will have different characteristics when compared with that of simple structures like $\Gamma_a(t)$ and $\Gamma_c(t)$ when applied to the IIR-MPF.

2.2 Coherence management of multi-longitudinal-mode lasers in IIR-MPF

From Eq. (3), the weighting of each phase sensitive cross-term with specified m and n in the response of IIR-MPF is determined by the factor $K_m K_n \Gamma[(n-m)T]$. Managing the coherence of source to minimize all $K_m K_n \Gamma[(n-m)T]$ terms is the key issue in the design of IIR-MPF. For sources with single peak on the $\Gamma(t)$ functions, e.g. $\Gamma_a(t)$ and $\Gamma_c(t)$, the factors $K_m K_n \Gamma[(n-m)T]$ can be neglected if the conditions $1/\nu_l \ll T$ or $1/\nu_s \ll T$ are satisfied respectively. But the linewidth of single mode laser ν_l is normally at or less than MHz level which limits the free spectral range (FSR = $1/T$) of the IIR-MPF to lower than MHz. For the filtered white noise source with $\Gamma_c(t)$, the ν_s can be much larger than GHz level which avoids the limitation to the FSR. However, the low intensity and low power efficiency of the filtered white noise limit the application of such sources in IIR-MPFs. In this Section, we will utilize coherence management of MLM lasers to design stable IIR-MPF with GHz level FSR.

We set the target of the FSR of the IIR-MPF to 1 GHz and the corresponding time delay T of the tap generator is 1 ns. First we consider a passive fiber loop as the tap generator. The amplitude factor of the p-th tap K_p is $(1-R)^{1/2}$ when p = 1 and $R(1-R)^{(p-2)/2}$ when $p > 1$ where R is the power coupling ratio of the coupler to fabricate the fiber loop. To demonstrate the use

#227130 - $15.00 USD Received 18 Nov 2014; revised 30 Jan 2015; accepted 1 Feb 2015; published 11 Feb 2015

of coherence management to suppress the factors $K_mK_n\Gamma[(n-m)T]$, we first consider the combinations of $m = 0$, and $n = 1, 2, \ldots\infty$ without loss of generality. Since the linewidth ν_l is normally much smaller than the mode spacing $\Delta\nu$, if the filter taps do not last longer than $1/\nu_l$, we can assume $\nu_l = 0$ corresponding to a flat envelope of the peaks of $\Gamma_b(t)$.

Figure 3 shows the process of the coherence engineering with $R = 0.5$, where the dashed red lines, solid blue curves, and the red bars represent the intensity of K_mK_n, $\Gamma[(n-m)T]$ and $K_mK_n\Gamma[(n-m)T]$ versus the time delay $(n-m)T$ respectively. We set an intensity threshold of −100 dB. Taps with intensity below the threshold are neglected. In Fig. 3(a), the MLM laser has spectral bandwidth $\nu_s = 250$ MHz and mode spacing $\Delta\nu = 50$ MHz. It is clear that multiple phase sensitive coherent taps indicated by the red bars are not suppressed. The first tap, which is also the maximal tap at $(n-m)T = 1$ ns has intensity −7 dB. These coherent taps will hence introduce large fluctuations on the response of the IIR-MPF. To suppress the coherent taps in Fig. 3(a), a straight forward method is to increase the bandwidth of the MLM laser which will reduce the duration of each peak in $\Gamma_b(t)$ as shown in Fig. 3(b), where the bandwidth $\nu_s = 2$ GHz is used. In Fig. 3(b), all the taps in the first peak are suppressed and the first coherent tap appears at $(n-m)T = 20$ ns with intensity −33 dB. Compared with Fig. 3(a), the coherent taps in Fig. 3(b) have much smaller intensities, which will reduce the fluctuation on the response of IIR-MPF. Another route to suppress the coherent taps is to reduce the mode spacing $\Delta\nu$ which will increase the period of $\Gamma_b(t)$ and hence reduce the number of peaks lcoated in the region $K_mK_n > -100$ dB. The result with $\Delta\nu = 15$ MHz and $\nu_s = 250$ MHz is shown in Fig. 3(c). If the mode spacing $\Delta\nu = 15$ MHz and the bandwidth $\nu_s = 2$ GHz, all the coherent taps can be suppressed to lower than −100 dB as shown in Fig. 3(d). It should be pointed out that in Figs. 3(a) and 3(b), the period of the $\Gamma_b(t)$ is an integral multiple of the fiber loop time delay T. If the value of $1/\Delta\nu$ is not an integral multiple of T, then some of the peaks of $\Gamma_b(t)$ will not overlap with any red bars because of Vernier effect. This will effectively reduce the total intensity of the residual coherent taps, especially when the pulses in $\Gamma_b(t)$ are very narrow.

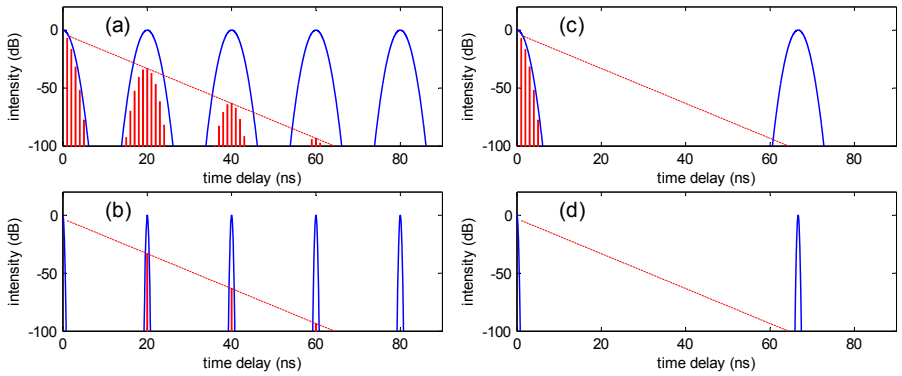

Fig. 3. The intensities of the factors K_mK_n (red dashed lines), $\Gamma[(n-m)T]$ (blue solid curves) and $K_mK_n\Gamma[(n-m)T]$ (red bars) versus time delay $(n-m)T$ with (a) $\nu_s = 250$ MHz, $\Delta\nu = 50$ MHz, (b) $\nu_s = 2$ GHz, $\Delta\nu = 50$ MHz, (c) $\nu_s = 250$ MHz, $\Delta\nu = 15$ MHz, and (d) $\nu_s = 2$ GHz, $\Delta\nu = 15$ MHz.

To quantify the weighting of the residual $K_mK_n\Gamma[(n-m)T]$ terms in Eq. (3) with different $\Delta\nu$ and ν_s, we will calculate the summation of all $K_mK_n\Gamma[(n-m)T]$ terms with all combinations of m and n when $m \neq n$. From Fig. 3, the mode spacing $\Delta\nu$ should be small enough to push all the peaks of $\Gamma_b(t)$ out of the range of the large K_mK_n taps. But the range of the K_mK_n taps will increase with the enhancement of the Q factor of the IIR-MPF. To investigate the impact of the Q factor to the stability, a passive fiber loop with $R = 0.5$ and $R = 0.2$, and a high Q loop with $K_n = 0.99^{(n-1)}$ are characterized. The intensities of the summations are indicated by the

#227130 - $15.00 USD Received 18 Nov 2014; revised 30 Jan 2015; accepted 1 Feb 2015; published 11 Feb 2015

color maps and contour lines in Fig. 4. All the values of $1/\Delta\nu$ are chosen as integral multiple of T. The ordinate $\Delta\nu$ and abscissa ν_s are normalized to the fiber loop FSR by multiplying the fiber loop delay T. The ordinate is in logarithmic scale. From Fig. 4, the analysis based on Fig. 3 is confirmed that the coherent taps can only be suppressed when the conditions for bandwidth and mode spacing are both satisfied. From Fig. 4(a), the impact of $\Delta\nu$ and ν_s are nearly independent. For example, if $\nu_s = 1.35/T$, the intensity will decrease rapidly when $\Delta\nu$ decreases from $1/T$, but the rate of decrease will slow down when the $\Delta\nu$ is smaller than $0.05/T$. The intensity stops decreasing at –30 dB even if $\Delta\nu$ decreases further. This can also be observed when we fix $\Delta\nu$ and vary ν_s. Each value of $\Delta\nu$ or ν_s corresponds to a minimum value of the intensity. When the tap generator changes to the fiber loop with $R = 0.2$, as shown in Fig. 4(b), a smaller $\Delta\nu$ than that with $R = 0.5$ is required to suppress the intensity to the same value. Decreasing the coupling ratio will reduce the coupling loss of the light in the fiber loop and increase the number of filter taps which will then increase the Q factor [2]. The increased tap number will require smaller $\Delta\nu$ to reduce the pulse number of $\Gamma_b(t)$ that locates within the tap duration. To further increase the Q factor of the IIR-MPF, amplified fiber loop or other high Q resonators could be adopted [20–25]. In a high Q loop, the decay of K_n will be slow since the loss in each round trip is very small. Figure 4(c) shows the results with a high Q loop where the amplitude $K_n = 0.99^{(n-1)}$. If we want to suppress the residual terms to –30 dB, $\Delta\nu$ should be less than $1.45 \times 10^{-3}/T$ which corresponds to a fiber cavity length ~140 m with T = 1 ns. Management of the laser coherence by increasing the fiber cavity length to ensure the stability of the high Q factor IIR-MPF is feasible until the loss of the required long fiber in the cavity cannot be compensated by the gain element.

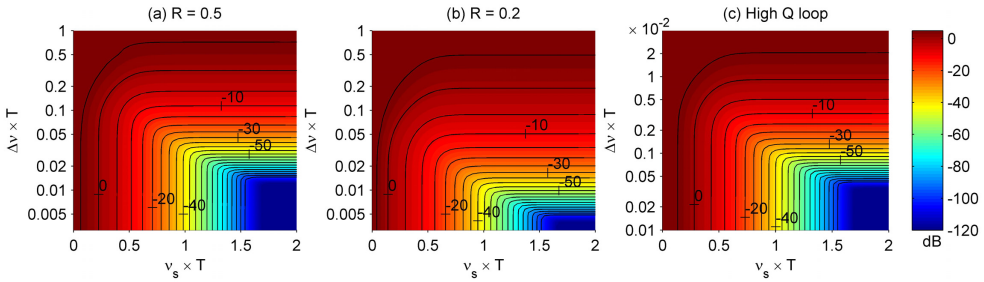

Fig. 4. The summation of $K_mK_n\Gamma[(n-m)T]$ with all m and n for phase sensitive terms. (a) and (b) adopt passive fiber loops with coupling ratio 0.5 and 0.2 respectively. (c) adopts a high Q loop, which can be an amplified fiber loop or a high Q resonator. The intensities of the summations are indicated by the color maps where contour lines with 5 dB spacing are also plotted.

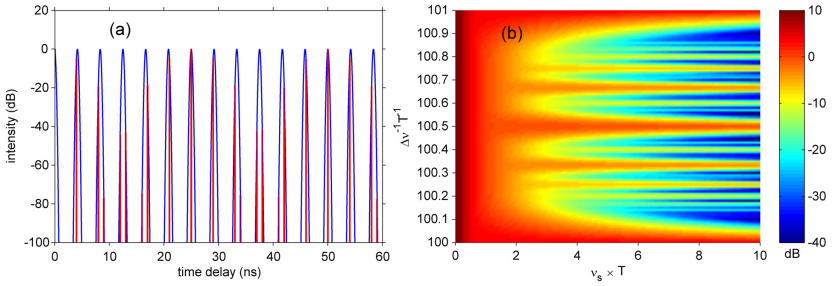

Fig. 5. (a) An example of the intensities of $\Gamma[(n-m)T]$ (blue solid curves) and $K_mK_n\Gamma[(n-m)T]$ (red bars) versus time delay $(n-m)T$ when the fiber is not an integral multiple of $\Delta\nu$. (b) The summation of $K_mK_n\Gamma[(n-m)T]$ terms with different $\Delta\nu$ and ν_s is indicated by the color map.

When the duration of the taps is sufficient long, increasing the fiber laser cavity length to suppress the coherent terms will no longer be possible. In this case, the linewidth of the lasing

#227130 - $15.00 USD Received 18 Nov 2014; revised 30 Jan 2015; accepted 1 Feb 2015; published 11 Feb 2015

modes cannot be assumed to zero since the duration of the taps will exceed the coherence time of an individual mode. Moreover, when the fiber laser cavity round trip time $1/\Delta\nu$ is not an integral multiple of the time delay T, part of the taps will be suppressed because of Vernier effect. Figure 5(a) shows an example of the tap suppression by Vernier effect. When the spectral bandwidth ν_s of the laser signal is large, the pulses on $\Gamma_b(t)$ will be very narrow. Slight mismatch between the period of $\Gamma_b(t)$ and the tap interval T will significantly suppress the amplitude of many coherent taps. Figure 5(b) shows the summation of the $K_m K_n \Gamma[(n-m)T]$, where $K_m = K_n = 1$ for all values of m and n, when we slowly tune $\Delta\nu^{-1}T^{-1}$ from 100 to 101 and vary $\nu_s T$ from 1 to 10. Here the linewidth of the lasing modes ν_l is set to $\Delta\nu/10$ from experience. From Fig. 5(b), with $\nu_s T < 2$, the varying of $\Delta\nu^{-1}T^{-1}$ will not significantly affect the intensity of the summation. But with $\nu_s T > 2$, the intensity can be greatly suppressed in many regions of the color map. With $\nu_s T = 10$, the intensity can be suppressed to less than −30 dB in large ranges of $\Delta\nu^{-1}T^{-1}$.

From the above analysis, by controlling the mode spacing $\Delta\nu$ and the spectral bandwidth ν_s of the MLM laser, the intensity of the coherent terms can be suppressed to a very low level to ensure the stability of the IIR-MPF with low or high Q factor. In most situations, the stability of the response of the IIR-MPF will be enhanced by reducing the mode spacing $\Delta\nu$ and/or increasing the spectral bandwidth ν_s. Even with extremely high Q loop, the stability can also be controlled by carefully engineering $\Delta\nu$ and ν_s based on Vernier effect.

3. Experimental realization of GHz level IIR-MPF

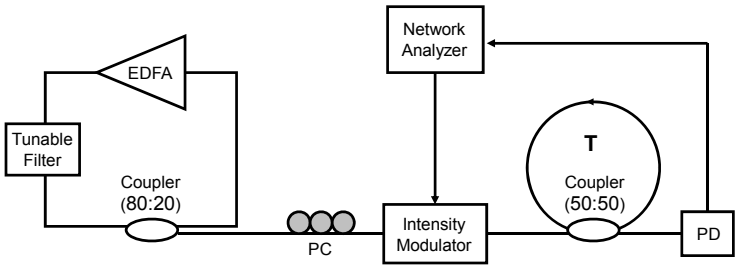

Fig. 6. Experimental setup of the IIR-MPF based on an MLM fiber laser.

From Section 2, an MLM laser with small $\Delta\nu$ and large ν_s will enable the fabrication of stable GHz level single source IIR-MPF. To experimentally confirm the analysis, an MLM fiber ring laser with an erbium doped fiber amplifier (EDFA) as the gain medium and a tunable filter to control the central wavelength and bandwidth is used as the source of a typical IIR-MPF as shown in Fig. 6. A network analyzer is used to generate the RF signal and detect the transmitted signal after the IIR-MPF. The RF signal is loaded to the optical signal by an intensity modulator. Two ports of a 50:50 coupler are spliced to form a fiber loop with ~0.35 m length to provide a time delay T ~1.7 ns for the IIR-MPF. Further decrease of the fiber loop length is limited by the fusion splicer we used. The loop length can be reduced further by other methods to fabricate the loop.

To illustrate the advantage of using an MLM fiber laser as the source of IIR-MPF, we compare the response of the IIR-MPF to that of utilizing DFB LD. Figures 7(a) and 7(b) show the output spectra of the MLM fiber laser and the DFB LD. The spectra are measured by a complex spectrum analyzer with resolution 1 MHz. We observe the MLM structure. The 3dB bandwidths of the DFB LD and the MLM fiber laser are 0.68 pm (~85 MHz) and 14.1 pm (~1.76 GHz) respectively. The coherence length calculated by $1/\nu_{3\text{-dB}}$ of the DFB LD is ~12 ns which is much longer than the time delay T. On the contrary, the coherence length of the MLM fiber laser ~0.57 ns is much shorter than T. Figures 7(c) and 7(d) show the response spectra of IIR-MPFs based on the DFB LD and the MLM fiber laser respectively. The IIR-

#227130 - $15.00 USD Received 18 Nov 2014; revised 30 Jan 2015; accepted 1 Feb 2015; published 11 Feb 2015

MPF based on the MLM fiber laser shows much better performance than that with the DFB LD. The measured FSR of the IIR-MPF response is 0.59 GHz.

As discussed in Section 2.2, although the IIR-MPF based on MLM fiber laser can achieve better response spectrum than that with DFB LD, the coherence of the MLM fiber laser should be managed by controlling the spectral bandwidth and longitudinal mode spacing to guarantee the stability of the IIR-MPF. To characterize the stability of the response of the IIR-MPF, with each parameter set, the response spectra are measured 20 times in 1 minute and plotted together which will straightforwardly indicate the stability. Furthermore, the standard deviations of the relative fluctuation of the response at every frequency Ω are measured using the 20 curves. Then the effective standard deviation ΔI_r is calculated by the average of the standard deviations on the range $0 < \Omega < 5$ GHz to quantitatively estimate the fluctuation of the whole response curve.

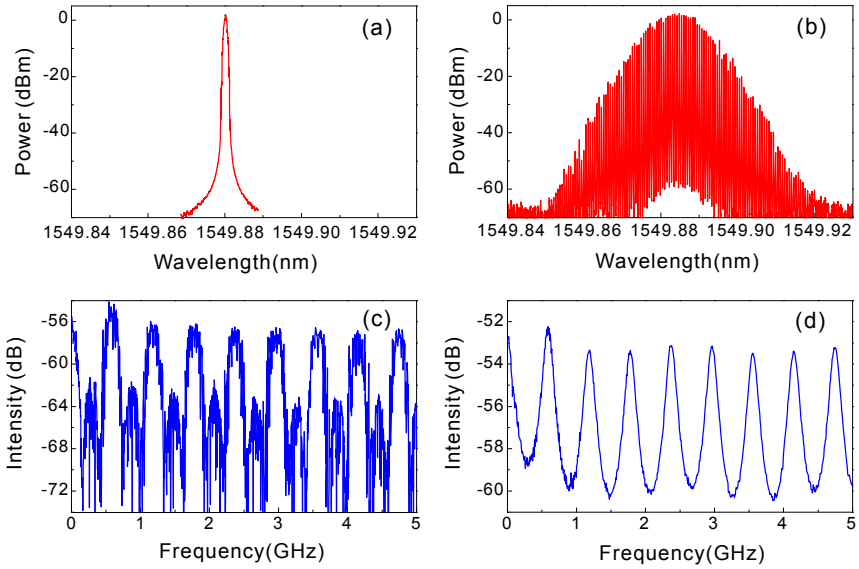

Fig. 7. (a) and (c) are the optical spectrum and response curve of the IIR-MPF with DFB LD as the source, respectively. (b) and (d) are the optical spectrum and response curve of the IIR-MPF with MLM fiber laser as the source, respectively.

First, the impact of the longitudinal mode spacing Δν is investigated as shown in Fig. 8. The fiber laser cavity is first set to ~3 m and Δν is ~72 MHz. Figures 8(a) and 8(c) show the optical spectrum and the response spectra of the IIR-MPF which are sampled 20 times in 1 minute. To reduce the mode spacing, a fiber with ~1 km length is inserted into the fiber laser cavity. The reduced mode spacing is less than 0.2 MHz and the corresponding period of the $\Gamma(t)$ function is more than 5 μs. The corresponding optical spectrum and the 20 response spectra sampled in 1 minute are shown in Figs. 8(b) and 8(d) respectively. From Figs. 8(c) and 8(d), the fluctuations observed on the response curves with the short cavity are significantly suppressed in the long cavity scheme in accordance with the prediction in Figs. 3 and 4. From the 20 plots in each figure, ΔI_r of the response curves with short cavity and long cavity are calculated as 6.9% and 2.0% respectively. From Fig. 8, the main to secondary sidelobe ratio (MSSR) is ~8 dB because the coupling ratio of the coupler is chosen as 0.5 which corresponds to an MSSR of 9.5 dB in ideal case [28]. The maximal MSSR of the IIR-MPF with passive fiber loop can be obtained with $R = 0.33$. It can be expected that if an amplified fiber loop is used, the number of taps and hence the Q factor can be significantly increased [20–24]. Another desirable and promising candidate of the tap generator in IIR-

#227130 - $15.00 USD Received 18 Nov 2014; revised 30 Jan 2015; accepted 1 Feb 2015; published 11 Feb 2015

MPF is a filter based on waveguides, such as microring resonators, which can show very high fineness and are very attractive to be used in IIR-MPF to achieve high Q factor [25, 26].

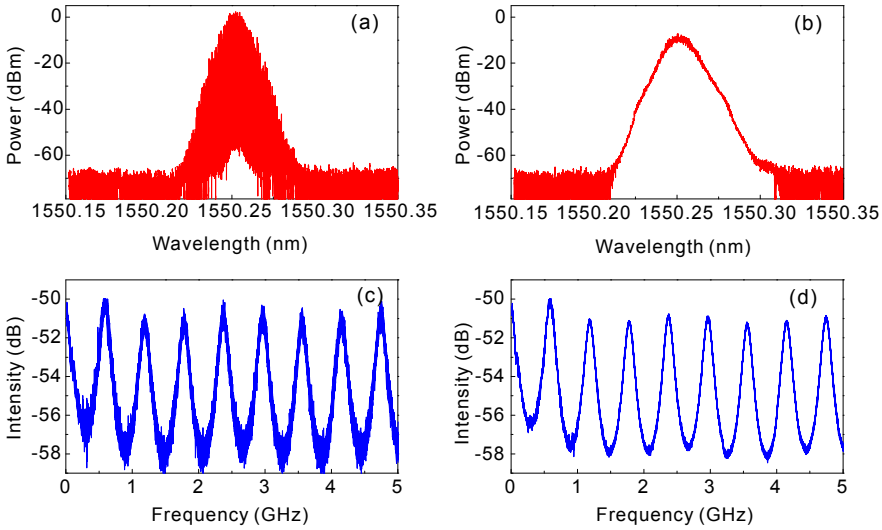

Fig. 8. (a) and (c) are the optical spectrum and response curve of the IIR-MPF with short cavity MLM fiber laser as the source, respectively. (b) and (d) are the optical spectrum and response curve of the IIR-MPF with long cavity MLM fiber laser as the source respectively. The response curves are sampled 20 times in 1 minute in each figure.

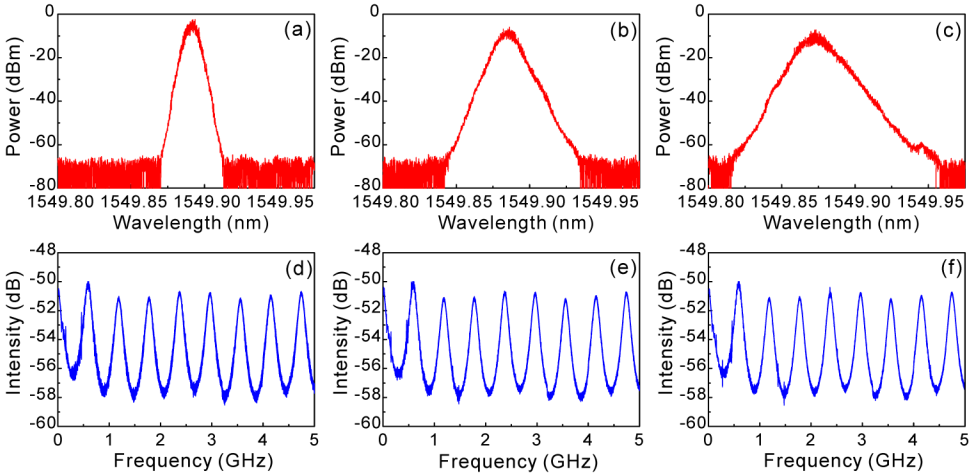

Fig. 9. (a), (b), and (c) are the optical spectra of the MLM fiber laser with bandwidth 5.9 pm (0.74 GHz), 13.7 pm (1.71 GHz), and 20.5pm (2.56 GHz), respectively. (d), (e), and (f) are the corresponding response curves of IIR-MPFs with the sources shown in (a), (b), and (c). The response curves are sampled 20 times in 1 minute in each figure.

Besides the mode spacing $\Delta\nu$, the spectral bandwidth ν_s is another crucial parameter of the proposed system. From previous work on IIR-MPF with single source, typically with single longitudinal-mode lasers, it is already known that the stability of the MPF depends significantly on the coherence length which is inversely proportional to the bandwidth. But in most single longitudinal-mode lasers, the bandwidth of the output is hard to control. In MLM fiber lasers, the spectral bandwidth of the output signal can be controlled easily by tuning the bandwidth of the bandpass filter. Figures 9(a), 9(b) and 9(c) are the spectra with bandwidth

#227130 - $15.00 USD Received 18 Nov 2014; revised 30 Jan 2015; accepted 1 Feb 2015; published 11 Feb 2015

5.9 pm (0.74 GHz), 13.7 pm (1.71 GHz) and 20.5pm (2.56 GHz), respectively. The fiber cavity length is the same as that in Fig. 8(b). Figures 9(d), 9(e) and 9(f) show the corresponding response curves of the IIR-MPF which are sampled 20 times in 1 minute in each figure, respectively. As expected, when the spectral bandwidth increases, the fluctuations of the response curve are reduced. The ΔI_r of the response curves in Figs. 9(d), 9(e) and 9(f) are 3.4%, 2.1%, and 1.8% respectively. It can be seen that although the fluctuation of the response curves are suppressed by increasing the spectral bandwidth of the laser, the rate of decrease will slow down when the spectral bandwidth is large. The residual fluctuation implies the existence of other noise sources such as thermal noise, and the amplitude noise of the lasing modes which is not considered here [2].

Tunability of the optical source can significantly improve the flexibility of the IIR-MPFs when applied into different systems especially WDM systems where reconfigurability is very important. In the proposed IIR-MPF system utilizing MLM fiber lasers, the central wavelength of the source can be tuned freely by adjusting the tunable filter. Such tuning is impossible with DFB LDs. Although such tunability is also available by applying the tunable filter to a white noise source such as SLD or ASE, but the filtered power is low and the power will vary greatly at different wavelengths because of the uneven spectra. To demonstrate the advantage of MLM fiber laser, Fig. 10 shows the output spectra of the laser and the corresponding response curves of the IIR-MPF when the central wavelength of the laser is varied within 20 nm. The power variation in the 20 nm tuning range is only ~3 dB and the response curve of the IIR-MPF at different wavelengths varies only slightly.

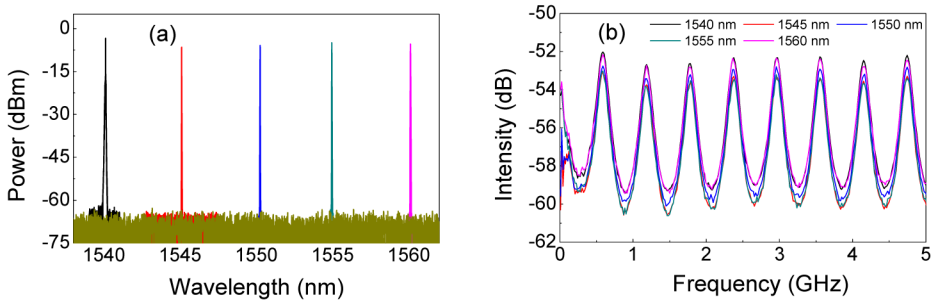

Fig. 10. (a) The optical spectra of the MLM fiber laser and (b) the corresponding response curves of the IIR-MPFs with different central wavelengths tuning from 1540 nm to 1560 nm.

From the above results, a stable single source IIR-MPF with an FSR of 0.59 GHz is realized in experiment. By management of the coherence of the MLM fiber laser, the relative fluctuation of the response curve can be optimized to less than 2%. The IIR-MPF system is reconfigurable by tuning the lasing wavelength of the laser and the response curve is also unchanged in the tuning. Such a reconfigurable IIR-MPF which is transparent to the RF signal is flexible in the integration to WDM systems. In this paper, we use a passive fiber loop to generate the filter taps. Because of the coupler loss, the intensity of the taps will be attenuated after every round trip in the loop so the Q factor of the IIR-MPF is limited. The Q factor is expected to be enhanced if an amplified fiber loop or high Q resonators are used. Furthermore, if a shorter cavity is used, the FSR can be enhanced to several GHz or even higher.

4. Conclusion

In this paper, we proposed to use an MLM laser as the source of IIR-MPF to fabricate stable GHz level MPF. It is the first time that an MLM laser is utilized in IIR-MPF. We analyze the response function of such IIR-MPF. The degree of coherence of the laser is studied. The degree of coherence of MLM laser shows a periodic structure which is significantly different to that of single mode lasers. We show that stable IIR-MPF with GHz level FSR can be

#227130 - $15.00 USD Received 18 Nov 2014; revised 30 Jan 2015; accepted 1 Feb 2015; published 11 Feb 2015

realized if the coherence of the laser is managed. Based on the theoretical analysis, we fabricated an IIR-MPF based on an MLM erbium doped fiber laser. The impact of the mode spacing $\Delta\nu$ is investigated by inserting a ~1 km fiber into the cavity. The influence of the bandwidth to the stability is investigated by tuning the bandwidth of the output spectrum. A stable IIR-MPF with an FSR of 0.59 GHz is realized and the relative fluctuation of the response curve is optimized to be less than 2%. Besides a stable response, the IIR-MPF is also reconfigurable by tuning the central wavelength of the laser in a range of 20 nm. Thus reconfigurable IIR-MPF with high Q factor and several GHz or higher FSR can be realized based on such MLM fiber laser when amplified and short fiber cavity are adopted.

Acknowledgments

This work was supported in part by the National Natural Science Foundation of China (NSFC) (61475065, 61475131), the Fundamental Research Funds for the Central Universities (No 21614606, 21612201) in China, and by the Hong Kong Research Grants Council (PolyU5263/13E, PolyU5272/12E), the Hong Kong Scholars Program 2013 (PolyU G-YZ45) of the Hong Kong Special Administrative Region of China.

#227130 - $15.00 USD Received 18 Nov 2014; revised 30 Jan 2015; accepted 1 Feb 2015; published 11 Feb 2015